Available online at www.sciencedirect.com
SCIENCE DIRECT®
Journal of Power Sources 141 (2005) 227–240
JOURNAL OF POWER SOURCES
www.elsevier.com/locate/jpowsour

Finite-volume modeling and hybrid-cycle performance of planar and tubular solid oxide fuel cells

Christoph Stiller*, Bjørn Thorud, Steinar Seljebø, Øistein Mathisen, Håvard Karoliussen, Olav Bolland

Department of Energy and Process Engineering, Norwegian University of Science and Technology, Kolbjorn Hejes vei 1B, Trondheim N-7491, Norway

Received 18 February 2004; received in revised form 14 July 2004; accepted 27 September 2004
Available online 23 November 2004

Abstract

The paper describes two 2D steady-state models for solid oxide fuel cells (SOFC) with planar and tubular geometries fuelled by methane. Following a description of the basic geometries and general premises the approaches, assumptions and simplifications for the calculation of ohmic resistance, convective, conductive and radiative heat transfer are given. The modeling approach of the chemical reactions and molar and thermal balances are depicted in detail with the intention to allow for reproduction of the models. The required boundary conditions and input parameters of the models are also discussed. Relying on models, a bottoming GT cycle is introduced and specified and a base case for operation defined. The influence of pressure ratio, air inlet temperature, air flow rate and anode gas recycling are investigated in a parameter study. For both designs air flow rate and pressure ratio are the most important parameters considering the system performance, but for the tubular system these parameters have less impact than for the planar design. Based on the parameter study, a near-optimum case is defined specifically for both systems and the conditions in the fuel cells are investigated. The cycle balance is different in both systems, as the tubular fuel cell requires a lower air inlet temperature. Both fuel cell systems achieve above 65% electric efficiency.

Keywords: SOFC; Tubular; Planar; Model; Hybrid

1. Introduction

Combined solid oxide fuel cells and gas turbine (SOFC)/GT cycles promise to achieve high electric efficiencies even for small-scale systems with power output below 10 MW and hence have a certain potential in decentralized power generation concepts. However, there is a lot of uncertainty about the best layout of the fuel cell and the hybrid cycle in terms of feasibility, performance, economics and controllability. This paper compares the performance of the two most common SOFC geometries, namely planar and tubular, in a gas turbine hybrid cycle. It describes the configuration of the fuel cells and gives a comprehensive and reproducible description of the approach, assumptions and methods used for the steady-state models of the different geometries. After a validation of the fuel cell models, their implementation into the gas turbine cycle simulation is described, and the performance of combined cycles with planar and tubular SOFCs are studied and compared. Departing from a base case, the sensitivities to certain process parameters are studied and discussed and operational options and constraints are derived. The maximum efficiency under near-optimum operation is estimated.

2. Fuel cell models

2.1. Fuel cell geometries and modeling premises

The investigated planar SOFC is a cross-flow, electrolyte-supported cell. A previously in-house developed repeat

Abbreviations: CV, control volume; FU, fuel utilization; GT, gas turbine; PEN, positive electrode–electrolyte–negative electrode; SOFC, solid oxide fuel cell; TIT, turbine inlet temperature

* Corresponding author. Tel.: +47 7359 3723; fax: +47 7359 8390.
E-mail address: Christoph.stiller@ntnu.no (C. Stiller).

0378-7753/$ – see front matter © 2004 Elsevier B.V. All rights reserved.
doi:10.1016/j.jpowsour.2004.09.019

Nomenclature

Symbols

A	area (m^2)
A_{act}	active cell area (m^2)
co	gas component
c_p	specific heat capacity ($J\,K^{-1}\,mole^{-1}$)
D_h	hydraulic diameter (m)
E^{rev}	reversible potential (V)
F	Faraday constant ($96485\,C\,mole^{-1}$)
I	total CV current (A)
J	lumped parameter
L	length (m)
n	molar flow ($mole\,s^{-1}$)
Nu	Nusselt number
p	pressure (Pa)
$\dot{Q}$	radiative heat flow (W)
R	universal gas constant ($8.314\,J\,K^{-1}\,mole^{-1}$)
r	radius (m)
$r_{...}$	reaction rate ($mole\,s^{-1}$)
$R_{1...}R_5$	heat resistivity of planar model building blocks (kW^{-1})
$R_{p,i}$; $R_{p,j}$	solid heat resistivity of planar model in i- and j-direction (kW^{-1})
$R_{t,ax}$	axial heat resistivity of tubular model (kW^{-1})
$R_{t1...}R_{t6}$	radial chain heat resistivity of tubular model (kW^{-1})
R_Ω	ohmic resistance (Ω)
T	temperature (K)
T_{black}	temperature of black body receiving radiation energy for the pre-reformer
U	cell voltage (V)

Greek letters

α	convective heat transfer coefficient ($W\,m^{-2}\,K^{-1}$)
δ	thickness (m)
ΔH	enthalpy change ($J\,mole^{-1}$)
ε	emissivity (0.8)
η	overpotential (V)
λ	heat conduction efficient ($W\,m^{-1}\,K^{-1}$)
ρ	specific resistance ($\Omega\,m$)
σ	Stefan–Boltzmann-constant ($5.67 \times 10^{-8}\,W\,m^{-2}\,K^{-4}$)

Indexes

a	anode
a_1	cathode air (tubular model)
a_2	injector air
air	air (planar)
c	cathode
co	gas component counter
e	electrolyte
electro	electrochemical reaction
f	fuel
i, j	counter for CV number in i- and j-direction
ic	interconnect
inj	injector
irrad	irradiation
p	planar
preref	pre-reformer
rad	radiation
ref	reforming reaction
s	solid (tube material)
shift	shift reaction
t	tubular

element geometry with a size of 3.8 mm × 3.8 mm [1] has been used as control volume. In order to scale the cell to the standard size of 100 mm × 100 mm, a matrix of 26 × 26 repeat elements is required. The resulting length of the cell is 98.8 mm. The tubular geometry is based on the current Siemens–Westinghouse technology [2], which is a cathode-supported, 1.5 m long and 22 mm diameter vertical tube. The air enters an inner tube (injector) from the top, is preheated while flowing downwards to the end of the tube where it turns and flows upwards between the cathode and the injector tube. The fuel is correspondingly fed from outside the tube and flows upwards. Fig. 1 shows the control volume of the planar and the tubular cell, together with the respective key dimensions and the materials. The tube interconnect that penetrates the anode and electrolyte is not shown here.

The following assumptions, simplifications and premises were chosen for the proposed models:

1. The fuel is partially pre-reformed methane.
2. Internal reforming at the anode. Kinetics of the reforming reaction are respected while the shift reaction is always at equilibrium.
3. A pre-reformer is thermally integrated by radiation from the edges of the cells for the planar design and radiation from the solid in the tubular design. The pre-reformer itself is not integrated in the SOFC model, but the required amount of heat is an input variable.
4. Single-cell setup is considered, i.e. adiabatic boundaries except the pre-reformer are assumed.
5. The electrochemical kinetics is limited to activation overpotential, i.e. no diffusion overpotential is calculated.
6. In the planar model, each CV has one temperature node respectively for solid, air and fuel temperature. The tubular model has additionally temperature nodes for the injector air and the injector tube.
7. Heat conduction is calculated in two dimensions in the planar model, neglecting heat flow in the stacking direction. The tubular model features heat conduction in axial direction as well as radiation between the concentric tubes.

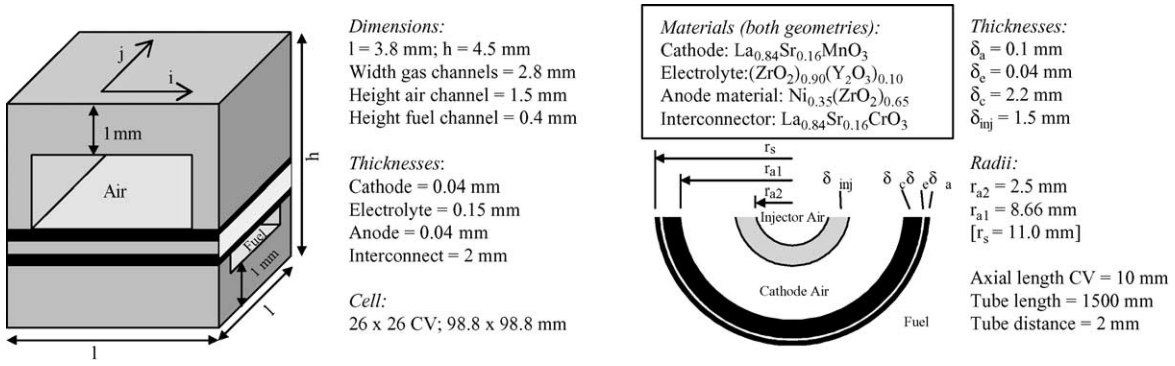

Fig. 1. Basic geometries of planar and tubular fuel cell control volume.

8. Radiation inside the planar cell is not included. In the tubular cell, radiation between the solid and the injector tube is modeled.

Similar work has been performed by Selimovic [3], Campanari [4] and some other SOFC researchers. The models present a common approach for finite-volume modeling of SOFC, detailed enough to give information about the internal behaviour of the cell and lean enough to be implemented into a hybrid system model and be solved within a reasonable calculation time.

2.2. Ohmic resistance

The ohmic resistance consists of the electronic current resistance in the interconnect and electrodes, and the ionic resistance in the electrolyte. The latter is the most dominating in both concepts.

In the planar model, the electronic resistance of anode, cathode and interconnect is low compared to the electrolyte resistance [5] and can be regarded as temperature independent within the given operating conditions. The material specific values for a temperature of 1173 K from Bossel [5] have been used to calculate the resistance of the layers. Conductivity and resistance for one CV as well as the temperature dependency of the electrolyte is listed in Table 1.

Even though in the tubular model, the same materials as for the flat plate model are applied, the properties given in literature are different due to unlike production techniques. Therefore, mostly temperature dependant resistances have been chosen for the tubular model. Also, the geometry is more complex than for the flat plate design. Although the tube is modeled in 2D, effects from current flowing in the 3rd direction (tangential) are accounted for by using the analytical expression for ohmic resistance of a control volume of the tube developed by Nisancioglu [6]. The expression is given in Eqs. (1)–(3), describing the so-called transmission line model. For further explanation, it is referred to the work of Niscanscioglu [6].

$$R_\Omega(\Omega) = L_{CV}\left(\frac{\left(\left(\frac{\rho_a}{\delta_a}\right)^2+\left(\frac{\rho_c}{\delta_c}\right)^2\right)\cosh(J_e)+\frac{\rho_a\rho_c}{\delta_a\delta_c}(2+J_e\sinh(J_e))}{2\left(\frac{1}{\rho_e\delta_e}\right)^{1/2}\left(\frac{\rho_a}{\delta_a}+\frac{\rho_c}{\delta_c}\right)^{3/2}\sinh(J_e)}+\frac{\sqrt{\rho_{ic}\delta_{ic}\left(\frac{\rho_c}{\delta_c}\right)}}{2\tanh(J_{ic})}\right) \quad (1)$$

where

$$J_e = \frac{L_e}{2}\sqrt{\frac{1}{\rho_e\delta_e}\left(\frac{\rho_a}{\delta_a}+\frac{\rho_c}{\delta_c}\right)} \quad (2)$$

and

$$J_{ic} = \frac{L_{ic}}{2}\sqrt{\frac{1}{\rho_{ic}\delta_{ic}}\frac{\rho_a}{\delta_a}} \quad (3)$$

with the terms $\rho_{ic}\delta_{ic} = 0.002\,\Omega\,cm^2$ (taken from Nisancioglu [6]); $\rho_e = 8.78\times10^{-3}\,e^{9165/T}\,\Omega\,cm$ (taken from Ota [7]); $\rho_a = 2.99\times10^{-3}\,e^{-1395/T}\,\Omega\,cm$ (taken from Ota [7]); $\rho_c = 7.99\times10^{-3}\,e^{601/T}\,\Omega\,cm$ (taken from Ota [7]); $L_{CV} = 1$ cm (axial length of CV); $L_e = 6.16$ cm (circumferential length of electrode); $L_{ic} = 0.6$ cm (circumferential length of interconnect) and the thickness δ to be taken from Fig. 1.

Table 1
Ohmic resistances for the planar model

Layer	Conductivity (S m^{-1})	CV resistance (Ω)
Anode	30.39×10^3	91.24×10^{-6}
Cathode	12.87×10^3	215.2×10^{-6}
Interconnect	3.11×10^3	44.53×10^{-3}
Electrolyte	$33.4\times10^3\,e^{(-10300/T)}$	$3.11\times10^{-4}\times e^{(10300/T)}$

Table 2
Nusselt numbers and hydraulic diameters

	Planar model		Tubular model			
	Air side	Fuel side	Inner air, injector	Outer air w.r.t. injector	Outer air w.r.t. cathode	Fuel, anode
Nu	4[a]	6.2[a]	4.36[b]	10[b]	7[b]	1.8[b]
D_h (mm)	1.953	0.7	5	9.328	9.328	11.3

[a] Taken from [10].
[b] Taken from [8].

2.3. Convective and conductive heat transfer

The heat transfer in the models is implemented by applying an electrical analogy, i.e. by calculation of thermal resistances.

The convective heat transfer coefficients α for all gas–solid interfaces are determined via the Nusselt number:

$$\alpha = \frac{Nu\lambda}{D_h} \tag{4}$$

The flow is assumed to be laminar and entrance effects have been neglected. Table 2 shows the Nusselt numbers *Nu* and hydraulic diameters D_h of the flow channels. Note that flow in annular ducts has different Nusselt numbers with respect to the inner and outer surface [8].

The heat conduction coefficients λ of the gases are calculated separately for the temperature and gas composition of each control volume using the polynomic formulae from Bossel [5] for each gas species.

Thermal conductivities of the solids are considered to be constant and their values are listed in Table 3.

The cells are assumed to operate under adiabatic conditions, thus heat conduction between adjacent cells is neglected. Only heat conduction between adjacent CVs, thus in *i*- and *j*-direction, is modeled. Due to its low thickness, the PEN structure is neglected in terms of heat conduction. For the heat transfer in *i*- and *j*-direction, the thermal resistance of a CV is calculated by dividing the interconnect into basic rectangular building blocks and calculating a total resistance of the circuit. The building block model, the resulting circuit in *i*-direction (*j* direction analogous) and the resulting total resistance equations are shown in Fig. 2.

In the tubular model, heat transfer in the radial direction is calculated by using an electrical analog circuit with conductive and convective resistances in series, shown in Fig. 3. The respective temperatures in the anode, electrolyte and cathode layer are regarded as uniform in each specific control volume. To calculate conduction into axial direction of the solid, the center temperature with respect to thermal resistance is chosen (i.e. the temperature at the radius where thermal resistance to inner and outer surface of the solid are equal). In

Table 3
Heat conduction coefficients

	Planar model	Tubular model			
	Interconnect	Anode	Electrolyte	Cathode	Injector
λ (W m^{-1}K^{-1})	3.5[a]	3[a]	2[a]	3[a]	6.84[b]

[a] Taken from [5].
[b] Taken from [10].

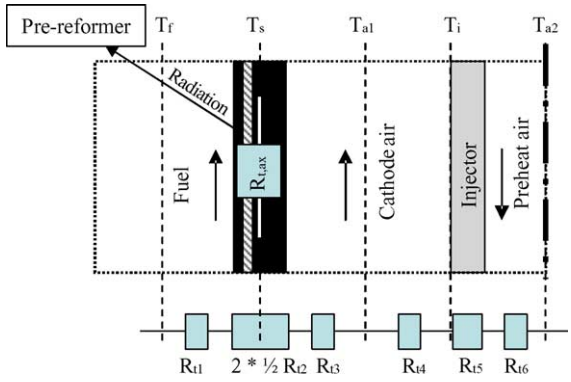

Fig. 3. Tubular radial heat conduction model.

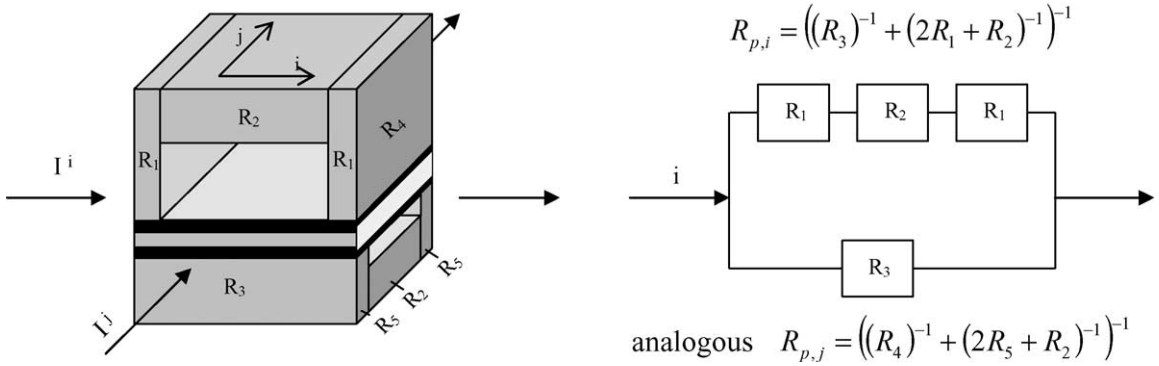

Fig. 2. Planar heat conduction model.

the injector tube, the outside temperature is used to calculate the radiation between injector and cathode. Axial heat conduction is only considered for the solid, not for the injector tube. The effect of interconnect and circumferential heat conduction is not considered.

2.4. Radiation

In order to reduce calculation time for the planar model, radiation between adjacent CVs was neglected. Even though the impact is lower than for the tubular model due to the small channel height, neglecting this phenomenon will according to Yakabe [9] lead to a steeper temperature profile and a shift of the maximum temperature upstream of the fuel flow. However, it is assumed that this effect does not seriously affect the key results, such as fuel utilization, efficiency and power output. Thus the model should still be able to produce reasonable results for use in combination with other processes, such as a gas turbine process. However, the energy demand of the pre-reformer is covered by radiation from the edges of the cell (i.e. the outermost CVs) towards a fictive black body with a uniform temperature. During the calculation, the black body temperature is adjusted iteratively until the radiative cell loss equals the pre-reformer duty. In order to be physically feasible, the black body temperature must be higher than or at least equal to the pre-reformer temperature.

The tubular geometry shows high temperature differences between the solid and the injector tube. Therefore, the tubular model includes radiation between the injector tube and the cathode. In this case, the control volumes of the tube represent a 10 mm high slice of the tube, and by pre-calculations it has been found that 95% of the radiative heat exchange occurs within the same CV and with the CVs lying above and underneath the CV in consideration. To reduce calculation time the remaining radiative heat exchange has been neglected. The implementation is shown in Fig. 1 with shape factors obtained from Incropera and Dewitt [10]. Note that the cathode has a shape factor of 34% to itself. Consequently only 66% of the radiation originating from the cathode occurs in the heat balance.

To reduce calculation time the pre-reformer heat duty is included as constant sink term in the tube solid heat balance, although this effect is of radiative character. Thus, all CVs deliver the same heat flow to the pre-reformer. To exclude a violation of the second law of thermodynamics, it is checked that the required temperature of the recipient for obtaining the required heat flow does not fall below the pre-reformer temperature.

2.5. Reactions and molar balances

Methane in the fuel is reformed at the entrance of the fuel cell in a reaction with steam, using nickel as catalyst:

$$CH_4 + H_2O \rightleftarrows CO + 3H_2 \tag{5}$$

The reaction rate of this reaction can, according to Rechenauer and Achenbach [11], be calculated by the following expression:

$$r_{CH_4}(\text{mole s}^{-1}) = 4274\,(\text{mole m}^{-2}\,\text{bar}^{-1}\,\text{s}^{-1})\,\text{e}^{-82\,(\text{kJ mole}^{-1})/RT}\,p_{CH_4}A_{\text{act}} \tag{6}$$

with the active area of $1.444 \times 10^{-5}\,\text{m}^2$ for the planar and $5.76 \times 10^{-4}\,\text{m}^2$ for the tubular CV. The carbon monoxide produced by methane reforming reacts with steam to form carbon dioxide and hydrogen:

$$CO + H_2O \rightleftarrows CO_2 + H_2 \tag{7}$$

At the SOFC operating temperature this reaction is very fast and assumed always to be in equilibrium. The equilibrium constant is determined with linear approaches for the Gibbs free energy found in standard literature. Due to a rather high steam to carbon ratio (~2–3) no carbon deposition is considered. A check whether this assumption is fair is however included.

Both carbon monoxide and hydrogen can theoretically participate in the electrochemical reactions, but for simplicity only the hydrogen reaction is considered.

$$H_2 + \tfrac{1}{2}O_2 \rightarrow H_2O \tag{8}$$

The reaction rate of the electrochemical reaction can be calculated by using the formulae (9)–(11):

$$U = E^{\text{rev}} - R_\Omega I - \eta \tag{9}$$

Table 4
Molar balance equations

Species	Planar model	Tubular model	Equation
CH_4	$n^{i,j}_{CH_4} = n^{i-1,j}_{CH_4} - r_{CH_4}$	$n^{i}_{CH_4} = n^{i-1}_{CH_4} - r_{CH_4}$	(26)
CO	$n^{i,j}_{CO} = n^{i-1,j}_{CO} + r_{CH_4} - r_{CO}$	$n^{i}_{CO} = n^{i-1}_{CO} + r_{CH_4} - r_{CO}$	(27)
CO_2	$n^{i,j}_{CO_2} = n^{i-1,j}_{CO_2} + r_{CO}$	$n^{i}_{CO_2} = n^{i-1}_{CO_2} + r_{CO}$	(28)
H_2	$n^{i,j}_{H_2} = n^{i-1,j}_{H_2} + 3r_{CH_4} - r_{H_2} + r_{CO}$	$n^{i}_{H_2} = n^{i-1}_{H_2} + 3r_{CH_4} - r_{H_2} + r_{CO}$	(29)
H_2O	$n^{i,j}_{H_2O} = n^{i-1,j}_{H_2O} - r_{CH_4} - r_{CO} + r_{H_2}$	$n^{i}_{H_2O} = n^{i-1}_{H_2O} - r_{CH_4} - r_{CO} + r_{H_2}$	(30)
O_2	$n^{i,j}_{O_2} = n^{i,j-1}_{O_2} - 0.5r_{H_2}$	$n^{i}_{O_2} = n^{i-1}_{O_2} - 0.5r_{H_2}$ (cathode air)	(31)
N_2	$n^{i,j}_{N_2} = n^{i,j-1}_{N_2}$	$n^{i}_{N_2} = n^{i-1}_{N_2}$ (cathode air)	(32)

$$\eta = 2.83 \times 10^{-4}\,(\Omega\,\mathrm{m}^2)\,\frac{I}{A_{\mathrm{act}}}\mathrm{e}^{8360\,(\mathrm{K})/T} \tag{10}$$

$$r_{\mathrm{H_2}} = \frac{I}{2F} \tag{11}$$

In Eq. (9) the current is calculated from a set operating voltage, open circuit potential, sum of the ohmic and ionic resistances and activation overpotential. The latter is approximated in Eq. (10), taken from Selimovic [3]. The reaction rate of H_2 can then be calculated by applying Faradays law as in Eq. (11). Being the most common approach for SOFC modeling, no diffusion overpotential has been regarded.

Applying these reactions and considering the gas flows into the CVs at anode and cathode side of the cell, the molar balance equations for all occurring species are determined as shown in Table 4.

2.6. Heat balances

In the planar model, heat balances are calculated for the air, fuel and solid (i.e. interconnect). Air flows in the *j*-direction, while fuel flows in the *i*-direction as depicted in Fig. 1.

Heat balance of the air is given by:

$$\alpha_{\mathrm{air}} A_{\mathrm{c}}(T_{\mathrm{air}}^{i,j} - T_{\mathrm{s}}^{i,j}) = \sum_{\mathrm{co}}^{\mathrm{co_{air}}}(c_{\mathrm{p,co}}(T_{\mathrm{air}}^{i,j-1})n_{\mathrm{co}}^{i,j-1}T_{\mathrm{air}}^{i,j-1} - c_{\mathrm{p,co}}(T_{\mathrm{air}}^{i,j})n_{\mathrm{co}}^{i,j}T_{\mathrm{air}}^{i,j}) \tag{12}$$

In words, the convective heat transport between air and solid material equals the sum of the heat capacity flows of all species into the CV minus the sum of the heat capacity flows of all species out of the CV.

The fuel heat balance is analogous; however, the fuel flows orthogonally to the air:

$$\alpha_{\mathrm{f}} A_{\mathrm{a}}(T_{\mathrm{f}}^{\mathrm{i,j}} - T_{\mathrm{s}}^{\mathrm{i,j}}) = \sum_{\mathrm{co}}^{\mathrm{co_f}}(c_{\mathrm{p,co}}(T_{\mathrm{f}}^{i-1,j})n_{\mathrm{co}}^{i-1,j}T_{\mathrm{f}}^{i-1,j} - c_{\mathrm{p,co}}(T_{\mathrm{f}}^{i,j})n_{\mathrm{co}}^{i,j}T_{\mathrm{f}}^{i,j}) \tag{13}$$

Due to the electrical analogy the heat balance in the solid is given by:

$$\begin{aligned}&\frac{2T_{\mathrm{s}}^{i,j} - T_{\mathrm{s}}^{i+1,j} - T_{\mathrm{s}}^{i-1,j}}{R_{\mathrm{p},i}} + \frac{2T_{\mathrm{s}}^{i,j} - T_{\mathrm{s}}^{i,j+1} - T_{\mathrm{s}}^{i,j-1}}{R_{\mathrm{p},j}} \\ &\quad + \alpha_{\mathrm{air}} A_{\mathrm{c}}(T_{\mathrm{s}}^{i,j} - T_{\mathrm{air}}^{i,j}) + \alpha_{\mathrm{f}} A_{\mathrm{c}}(T_{\mathrm{s}}^{i,j} - T_{\mathrm{f}}^{i,j}) \\ &= -r_{\mathrm{CH_4}}\Delta H_{\mathrm{ref}} - r_{\mathrm{CO}}\Delta H_{\mathrm{shift}} \\ &\quad - r_{\mathrm{H_2}}(\Delta H_{\mathrm{electro}} + 2UF) - \dot{Q}_{\mathrm{p,preref}}^{i,j}\end{aligned} \tag{14}$$

In words, the heat conduction in *i*- and *j*-direction plus the convection to air and fuel equals the heat conversion of reforming, shift and electrochemical reaction and the radiation to the pre-reformer. The latter is only different from zero at the edges of the cell (thus, $i = 1$, $i = 26$, $j = 1$ or $j = 26$) and where $T_{\mathrm{s}}^{i,j} > T_{\mathrm{black}}$ and is in these cases

$$\dot{Q}_{\mathrm{p,preref}}^{i,j} = \varepsilon\sigma A_{\mathrm{s}}((T_{\mathrm{s}}^{i,j})^4 - (T_{\mathrm{black}})^4) \tag{15}$$

with an emissivity of $\varepsilon = 0.8$. The tubular model is more complex, as it comprises three separate gas channels and furthermore includes radiation between the injector tube and the cathode.

The heat balance for the fuel is analogous to the planar model, however one-dimensional:

$$\frac{T_{\mathrm{f}}^{i} - T_{\mathrm{s}}^{i}}{R_{\mathrm{t1}}} = \sum_{\mathrm{co}}^{\mathrm{co_f}}(c_{\mathrm{p,co}}(T_{\mathrm{f}}^{i-1})n_{\mathrm{co}}^{i-1}T_{\mathrm{a}}^{i-1} - c_{\mathrm{p,co}}(T_{\mathrm{f}}^{i})n_{\mathrm{co}}^{i}T_{\mathrm{f}}^{i}) \tag{16}$$

The heat balance for the tube solid is extended by the radiation and irradiation terms and the pre-reformer duty:

$$\begin{aligned}&\frac{2T_{\mathrm{s}}^{i} - T_{\mathrm{s}}^{i+1} - T_{\mathrm{s}}^{i-1}}{R_{\mathrm{t,ax}}} + \frac{T_{\mathrm{s}}^{i} - T_{\mathrm{f}}^{i}}{R_{\mathrm{t1}} + \frac{1}{2}R_{\mathrm{t2}}} + \frac{T_{\mathrm{s}}^{i} - T_{\mathrm{a1}}^{i}}{R_{\mathrm{t3}} + \frac{1}{2}R_{\mathrm{t2}}} \\ &\quad + \dot{Q}_{\mathrm{s,rad}}^{i} - \dot{Q}_{\mathrm{s,irrad}}^{i} \\ &= -r_{\mathrm{CH_4}}\Delta H_{\mathrm{ref}} - r_{\mathrm{CO}}\Delta H_{\mathrm{shift}} - r_{\mathrm{H_2}}(\Delta H_{\mathrm{electro}} + 2UF) \\ &\quad - \dot{Q}_{\mathrm{t,preref}}\end{aligned} \tag{17}$$

where the radiative terms according to Fig. 4 can be expressed as:

$$\begin{aligned}\dot{Q}_{\mathrm{s,rad}}^{i} &= (0.3 + 2 \times 0.1 + 2 \times 0.08)\varepsilon\sigma A_{\mathrm{s}}(T_{\mathrm{s}}^{i})^4 \\ &= 0.64\varepsilon\sigma A_{\mathrm{s}}(T_{\mathrm{s}}^{i})^4\end{aligned} \tag{18}$$

and

$$\begin{aligned}&\dot{Q}_{\mathrm{s,irrad}}^{i} \\ &= \varepsilon\sigma[A_{\mathrm{inj}}(0.64(T_{\mathrm{inj}}^{i})^4 + 0.18(T_{\mathrm{inj}}^{i-1})^4 + 0.18(T_{\mathrm{inj}}^{i+1})^4) \\ &\quad + A_{\mathrm{s}}(0.1(T_{\mathrm{s}}^{i-1})^4 + 0.1(T_{\mathrm{s}}^{i+1})^4)]\end{aligned} \tag{19}$$

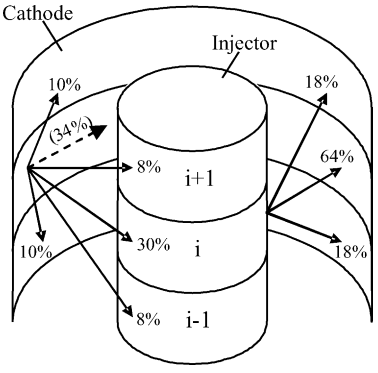

Fig. 4. Distribution of radiation energy between three adjacent control volumes in the tubular system.

with an emissivity of $\varepsilon = 0.8$. The pre-reformer duty $\dot{Q}_{\mathrm{t,preref}}$ is an input parameter, which must be determined externally to correspond with the pre-reformer inlet and outlet fuel composition enthalpies.

The heat balance for the cathode air between injector and cathode is:

$$\frac{T^i_{\mathrm{a1}} - T^i_{\mathrm{s}}}{R_{\mathrm{t3}} + \frac{1}{2}R_{\mathrm{t2}}} + \frac{T^i_{\mathrm{a1}} - T^i_{\mathrm{inj}}}{R_{\mathrm{t4}}} = \sum_{\mathrm{co}}^{\mathrm{co_{a1}}} (c_{\mathrm{p,co}}(T^{i-1}_{\mathrm{a1}}) n^{i-1}_{\mathrm{co}} T^{i-1}_{\mathrm{a1}} - c_{\mathrm{p,co}}(T^i_{\mathrm{a1}}) n^{\mathrm{i}}_{\mathrm{co}} T^i_{\mathrm{a1}}) \quad (20)$$

The heat balance for the injector tube is

$$\frac{T^i_{\mathrm{inj}} - T^i_{\mathrm{a1}}}{R_{\mathrm{t4}}} + \frac{T^i_{\mathrm{inj}} - T^i_{\mathrm{a2}}}{R_{\mathrm{t5}} + R_{\mathrm{t6}}} + \dot{Q}^i_{\mathrm{inj,rad}} - \dot{Q}^i_{\mathrm{inj,irrad}} = 0 \quad (21)$$

and again includes radiation and irradiation:

$$\dot{Q}^i_{\mathrm{inj,rad}} = (0.64 + 2 \times 0.18)\varepsilon\sigma A_{\mathrm{inj}} (T^i_{\mathrm{inj}})^4 = \varepsilon\sigma A_{\mathrm{inj}} (T^i_{\mathrm{inj}})^4 \quad (22)$$

and

$$\dot{Q}^i_{\mathrm{inj,irrad}} = \varepsilon\sigma A_{\mathrm{s}} (0.3(T^i_{\mathrm{s}})^4 + 0.08(T^{i-1}_{\mathrm{s}})^4 + 0.08(T^{i+1}_{\mathrm{s}})^4) \quad (23)$$

The gas composition in the injector is constant, as no reactions occur. Its heat balance is:

$$\frac{{T_{\mathrm{a2}}}^i - {T_{\mathrm{inj}}}^i}{R_{\mathrm{t5}} + R_{\mathrm{t6}}} = \sum_{\mathrm{co}}^{\mathrm{co_{a2}}} (c_{\mathrm{p,co}}({T_{\mathrm{a2}}}^{i+1}) n_{\mathrm{co}} {T_{\mathrm{a2}}}^{i+1} - c_{\mathrm{p,co}}({T_{\mathrm{a2}}}^i) n_{\mathrm{co}} {T_{\mathrm{a2}}}^i) \quad (24)$$

A check whether carbon deposition occurs can be included into the model by investigating the Gibbs energy of the reactions:

$$2\mathrm{CO} \rightleftarrows \mathrm{C} + \mathrm{CO_2} \text{ and } \mathrm{CH_4} \rightleftarrows \mathrm{C} + 2\mathrm{H_2} \quad (25)$$

If the Gibbs energy is less than or equal to zero, coking can theoretically occur. However, as the reactions are rather slow, small negative Gibbs energy values could possibly be tolerated. Nevertheless, Gibbs energy of zero was assumed to be the lower boundary for the carbon-deposition-free regime.

2.7. Boundary conditions and input parameters

The model requires temperature, pressure, composition and molar flow of the incoming gas streams as boundary conditions and therefore input parameters. The radiation heat from the cell edges to the pre-reformer is also a boundary condition which needs to be set according to the incoming (pre-reformed) fuel stream properties. This can be done by regarding the pre-reformer as a Gibbs reactor.

A further input parameter is the cell voltage, through which the current is determined by Eq. (9). The fuel utilization (FU), i.e. the fraction of fuel that is utilized by the fuel cell, is determined by evaluating Eq. (11) for each CV together with the solved heat balance equations.

In some cases it may be more desirable to define the fuel utilization instead of the operating voltage. This can be reached by a simple iteration routine, which modifies the voltage until the desired FU is reached. The electric current is a function of fuel flow, inlet concentration and fuel utilization and is thus also an implicit input parameter of the model.

In order to reduce calculation time both planar and tubular models do not consider special stacking particularities, i.e. except the specified heat exchange with the pre-reformer, the cell boundaries are adiabatic. This idealization means that indefinite stacks are modeled.

2.8. Numerical method and implementation

The implementation of the models results in a set of connected non-linear equations and some ancillary equations. The system is solved with the Newton–Raphson iteration procedure taken from Engeln-Muellges and Uhlig [12], which uses the partial derivatives of the equations to approach the solution.

The models have been implemented in Fortran 90, under the objective to integrate them into the flowsheet simulation software PRO/II by Simsci.

2.9. Type of results

The following results can be achieved with the SOFC models:

- Fuel utilization/voltage: depending on the running mode, one is an input parameter and the other one a result.
- Power output and global energy efficiency of the cell.
- Carbon deposition check: the CVs where carbon deposition is likely to occur.
- Black body temperature: the temperature an imaginary black body must have to receive the radiative heat flow that is required by the pre-reformer.
- Arrays of values for each CV (two-dimensional for the planar, one-dimensional for the tubular model)
  - Molar flow of all components.
  - Temperatures of air, fuel, solid (additional preheating air and injector for tubular model).
  - Temperature gradients in *i*- and *j*-direction of the planar and in axial direction of the tubular cell.
  - Electric current.
  - Molar amount of CO processed by the water gas shift reaction.

These results allow for a detailed study of the operation conditions of the fuel cells.

2.10. Model validation

The planar model has been validated against the models of Rechenauer [11] and Selimovic [3] using the input values of the IEA Benchmark Test [13]. The air and fuel flow rate were in both cases adjusted to the exact values selected by each compared model. The comparison in Table 5 shows that the planar model produces similar results in all shown parameters and a voltage deviation at identical fuel utilization and current density in the range of 2%.

The tubular model was validated using the experimental data and assumptions published by Campanari [4] for an atmospheric and a pressurized system. The input parameters and fuel utilization values of the experimental data have been simulated with the model, giving voltage and power as result. Input parameters and results are shown in Table 6. While the atmospheric case matches very well with a voltage deviation of only 0.8%, there is quite a high deviation in the pressurized case (13.3% in terms of voltage). However, the results are sensitive to the inlet temperature and fuel composition, which Campanari chose from a different work than the experimental results. If air and fuel inlet temperature for the model are increased by 90 K in case of the pressurized system, the voltage values match. As no complete set of input parameters and experimental results for tubular fuel cells was found in literature, we consider the exactness of the model as sufficient for the meanwhile. Once measurement data has been published, it is easy to calibrate the model to the data using parameter estimation.

Table 5
Validation of the planar model

	Rechenauer	Planar model	Selimovic	Planar model
Pressure (bar)	1	1	1	1
Fuel flow rate (mole s^{-1})	1.872×10^{-4}		1.784×10^{-4}	
Air flow rate (mole s^{-1})	3.047×10^{-3}		2.901×10^{-3}	
Inlet fuel and air temperature (K)	1173			
Fuel utilization (%)	85			
Inlet fuel composition (molar fraction)				
H_2	0.2626			
H_2O	0.4934			
CH_4	0.1710			
CO	0.0294			
CO_2	0.0436			
Voltage (V)	0.682	0.7	0.658	0.669
Voltage deviation (%)	2.64	2.64	1.67	1.67
Power (W)	20.46	21.12	19.74	19.02
Max. current density (A m^{-2})	4800	4570	6039	5798
Min. current density (A m^{-2})	1100	1260	804	1665
Max. solid temperature (°C)	1061	1036	1130	1063
Min. solid temperature (°C)	823	845	741	849
Max. temperature gradient (K mm^{-1})	7.09	8.95	n.a.	

Table 6
Validation of the tubular model

	Atmospheric (plant A)	Tubular model	Pressurized (plant B)	Tubular model
Pressure (bar)	1.05	1.05	3.5	3.5
Fuel flow per tube (mole s^{-1})	1.511×10^{-3}		2.287×10^{-3}	
Air flow per tube (mole s^{-1})	1.055×10^{-2}		1.290×10^{-2}	
Inlet fuel temperature (K)	823		860	
Inlet air temperature (K)	1104		1048	
Fuel utilization (%)	69		69	
Inlet fuel composition (molar fraction)				
H_2	0.258		0.226	
H_2O	0.284		0.334	
CH_4	0.11		0.131	
CO	0.057		0.057	
CO_2	0.228		0.241	
N_2	0.063		0.011	
Voltage (V)	0.69	0.695	0.639	0.564
Voltage deviation (%)	0.72	0.72	13.3	13.3
Power (W)	104.8	105.6	157.0	138.6

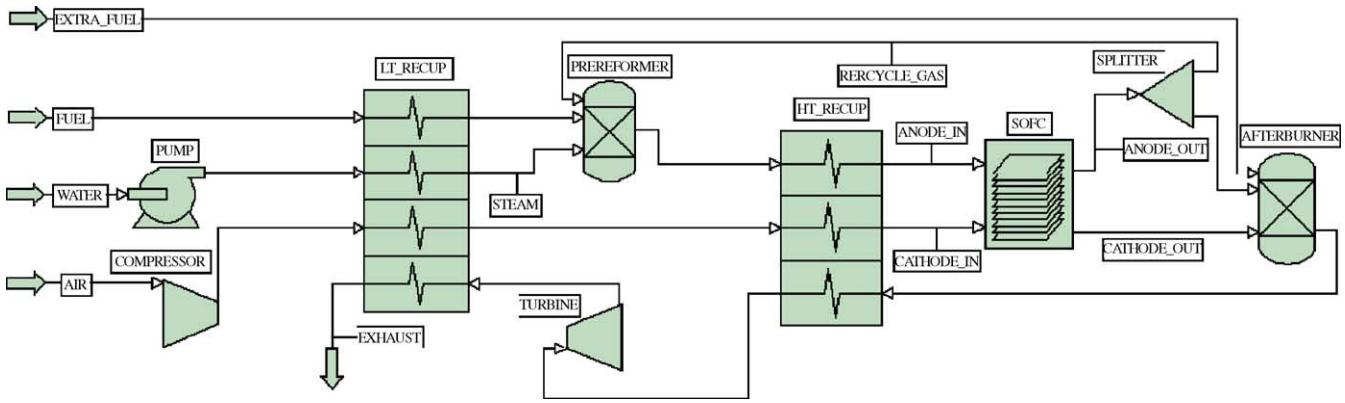

Fig. 5. Applied gas turbine cycle.

3. Hybrid cycle performance simulation

3.1. SOFC/GT cycle design and simulation premises

The modeled SOFC/GT cycle is illustrated in Fig. 5. The GT cycle and balance of plant equipment is implemented in PRO/II, where Fortran-based SOFC models are implemented as a user added subroutine in the flowsheet. The gas streams of the SOFC are defined by linking of the SOFC model in the flowsheet. The heat duty to the pre-reformer as well as voltage respectively fuel utilization of the SOFC models are entered via an entry form and can also be linked to process variables. Methane is partially reformed in a pre-reformer, which is modeled as a Gibbs reactor and thermally connected to the fuel cell. The operation temperature of the pre-reformer is controlled to equilibrium temperature of the desired pre-reforming level.

The cycle comprises two-stage cascaded heat recuperation, anode gas recycling and an afterburner for the unspent and possibly additional fuel. The pressure of the recycle gas is raised to the fresh fuel gas level by an ejector (not displayed). Losses in the ejector are not included in the energy balance of the system, as the fuel is assumed to be delivered directly from a high-pressure grid.

Table 7 summarizes the setup of the GT cycle. Most assumptions were taken from Pålsson [14]. The specifications that are most significant for the cycle or subject to changes during the parameter studies are shown below in Table 8.

The fuel cell input parameters, such as gas composition, pressure and temperature of the streams ANODE_IN and CATHODE_IN (Fig. 5) and the duty of the pre-reformer, are calculated in the PRO/II model and sent to the Fortran submodule. The solver operation mode and one further input parameter (operation voltage or fuel utilization level) must be specified in the SOFC module itself to be transferred to the Fortran routine.

The most important operational constraints for the planar SOFC are the maximum allowable temperature (T_{max}) of 1300 K [3] and the maximum temperature gradient in the area of 5 K mm^{-1} [11] to avoid thermal cracking of the cell. The tubular SOFC is less sensitive to this effect since the tubes can expand freely and the temperature is more uniform. Another issue is to avoid operational modes where coking can occur.

Table 7
GT cycle setup

Item (Fig. 5)	Specification
EXTRA_FUEL	100% Methane; 288 K/20 bar
AIR	288 K/1 bar
WATER	283 K/1 bar
COMPRESSOR	81% Adiabatic efficiency
TURBINE	84% Adiabatic efficiency; outlet pressure 1.1 bar
PRE-REFORMER	Gibbs reactor; pressure drop 2%; operating temperature 800–900 K (controlled to achieve desired pre-reforming degree); heat demand supplied by fuel cell
AFTERBURNER	Gibbs reactor; pressure drop 5%; complete combustion; coupled with HT_RECUP for heat transfer
SOFC	User added subroutine; pressure drop 2%; radiative heat loss is the PRE-REFORMER heat demand; specification of either operating voltage or fuel utilization
LT_RECUP	Pressure drop 2% for inlet air and exhaust (rest 0); cold products outlet 50 K below hot product inlet (1st and 2nd law check)
HT_RECUP	Pressure drop cold side 2% (hot side is coupled with AFTERBURNER), cold product temperature specified (fuel cell specifications)

Table 8
Base case parameters

Parameters	Planar	Tubular
Pressure (bar)	3	3
Steam to carbon ratio[a]	2.5	2.5
Fuel utilization (%)	85	85
Recirculation degree (%)	0	0
Fuel inlet temperature (K)	1123	1123
Air inlet temperature (K)	1123	923
Fuel flow per active cell area (mole m^{-2} s^{-1})	4.5×10^{-3}	3.8×10^{-3}
Air excess ratio, λ	6	4
Pre-reforming degree (%)	30	50

[a] Molar flow of steam divided by molar flow of methane in the fresh fuel entering the pre-reformer.

Table 9
Operational data at base case

System	Parameter	Planar system	Tubular system
Fuel cell	Efficiency (LHV, %)[a]	62.5	52.5
	Voltage[b] (V)	0.700	0.616
	Max. temperature (K)	1272	1130
GT cycle	TIT (K)	747	1185
	Spec. turbine power production[c] (%)	55	69
	Spec. compressor power consumption[c] (%)	48	37
SOFC/GT cycle	Total efficiency (LHV, %)	58.5	63.1

[a] Based on the fuel taking part in the electrochemical reaction.
[b] Voltage is a result of the model when a certain fuel utilization is determined.
[c] Ratio between power of compressor/turbine and fuel cell power.

3.2. Setup of a base case

As a starting point for parameter variations, a base case is defined. Table 8 shows the base case assumptions for the parameters that are of high importance for the cycle thermodynamics and fuel cell operation. The values represent typical values for SOFCs. A recirculation degree of zero has been chosen for calculation time reasons. Due to the nature of the different designs, some values differ for the planar and tubular model:

- The air inlet temperature of the tubular fuel cell lies well below the one of the planar SOFC in order to achieve the designated internal cooling effect of the preheating injector air.
- The fuel flow rate has been adapted geometry-specifically (i.e. fuel flow per m^2 s) in order to achieve comparable points in the operation ranges of the fuel cells. A value from Rechenauer [11] was chosen for the planar cell and a value from Yi [15] for the tubular cell.
- The tubular model is known to tolerate lower air excess ratios due to the ability of the tubes to tolerate higher thermal gradients by expanding freely. Therefore an air excess of 4 has been chosen for the tubular model.
- The pre-reforming degree of the tubular cell must be comparably high due to problems with the convergence of the model.

Table 9 shows main operational data of the fuel cell and the GT cycle for the base case. The listed fuel cell efficiency is based on the fuel taking part at the electrochemical reaction, i.e. without considering the fuel utilization. Power production and consumption by the gas turbine and compressor is given specifically as percentage of the fuel cell stack power. The power supplement of the GT cycle in relation to the fuel cell can thus be seen as the difference between specific turbine and compressor power. It is visible that in the planar system, the net power output from the GT cycle is very low and the system efficiency is below the fuel cell efficiency. This is mainly due to the low turbine inlet temperature. The tubular fuel cell has a lower efficiency due to the higher ohmic resistance, which leads to a higher heat production. The additional amount of heat is however spent on internal preheating of the incoming air flow. This in turn reduces the duty of the high temperature recuperator, which leads to a higher turbine inlet temperature (TIT) and therewith a higher output of the GT cycle.

3.3. Parameter study

A parameter study was performed by varying only one parameter at a time while keeping the others at their base case values. Figs. 6 and 7 shows the system efficiency for the planar design (left) and the tubular design (right) as a function of the varied parameters. The *y*-axis covers the same range

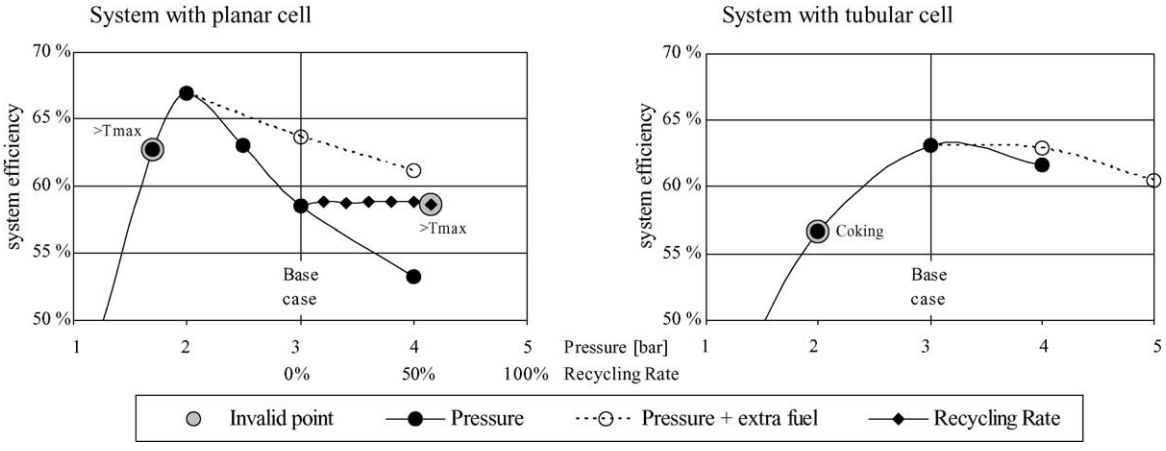

Fig. 6. Dependency of system efficiency on pressure and recycling rate.

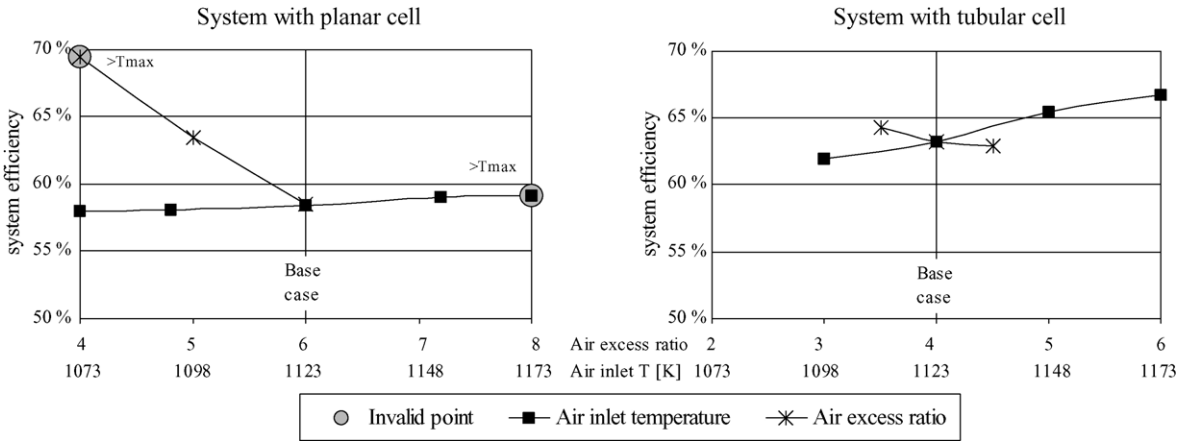

Fig. 7. Dependency of system efficiency on air inlet temperature and air excess ratio.

of values for all diagrams. The *x*-axis has been designed to show the base case value of each parameter and system in the middle, while the gradient is the same for each parameter. Figs. 8 and 9 show the gas turbine cycle power supplement to the fuel cell power in the same manner.

As can be seen from the bold line of Fig. 8, the turbine power output of the planar system decreases strongly at a pressure higher than 2 bar. That is because the TIT decreases due to a shift of the heat recovery duty towards the high-temperature recuperator. This can be countered by adding extra fuel to the afterburner. The dashed line in Figs. 6 and 8 shows the performance at a TIT controlled to 1173 K by this method. It can be seen that the power production of the planar system can be strongly increased at the cost of only a slight decrease in efficiency by adding extra fuel. For the tubular system, this effect is also present, however it is weaker. The system power output is furthermore increased slightly by the fuel cell efficiency increase at higher pressure.

Reducing the air flow rate would cause a high gain in efficiency of the planar system due to reduced heat and energy losses (see Fig. 6, left). However, the high excess air is required for cooling reasons, hence the maximum temperature is exceeded for an air excess ratio of 4. The tubular cell has better internal heat management and can thus be operated at a lower air excess ratio. This fact compensates for the lower efficiency of the tubular SOFC stack.

The air inlet temperature strongly influences the average temperature in the cell. Thus, a higher air inlet temperature has a positive influence on the reaction kinetics and results in higher fuel cell efficiency. This causes the tubular system efficiency to increase with increasing fuel cell air inlet temperature as can be seen in Fig. 7. In the planar system, this effect is partially compensated by the decreasing TIT caused by a higher heat transfer in the high-temperature recuperator. Regarding the internal temperature charts of the fuel cell, it turns out that the maximum local temperature of the SOFC can be effectively controlled by the air inlet temperature.

The influence of the recycling rate on the planar system efficiency is rather low. However it should be mentioned that anode gas recycling rate has practical advantages as it reduces the system complexity by providing steam and also decreases internal temperature gradients of the fuel cell. The recycling rate could not be checked in the tubular case due to solver stability reasons, but the same tendency could be expected.

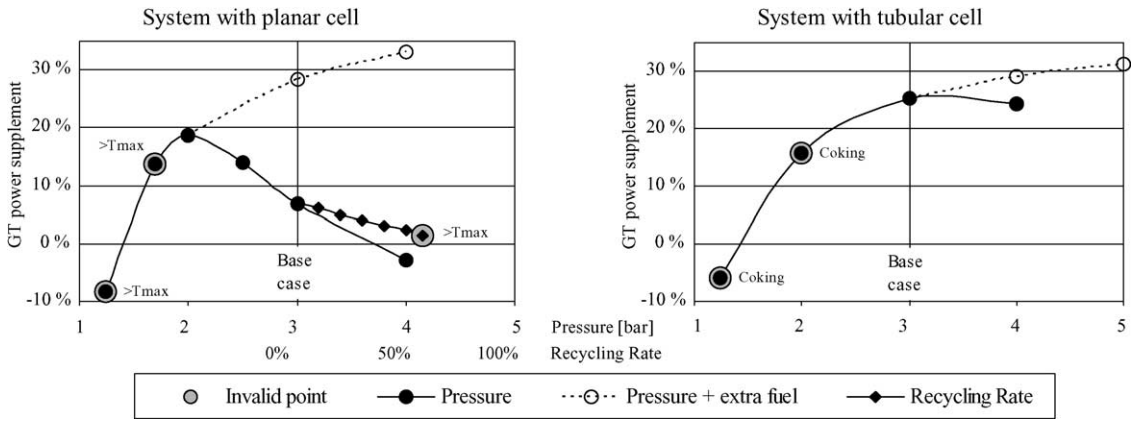

Fig. 8. Dependency of gas turbine power supplement on pressure and recycling rate.

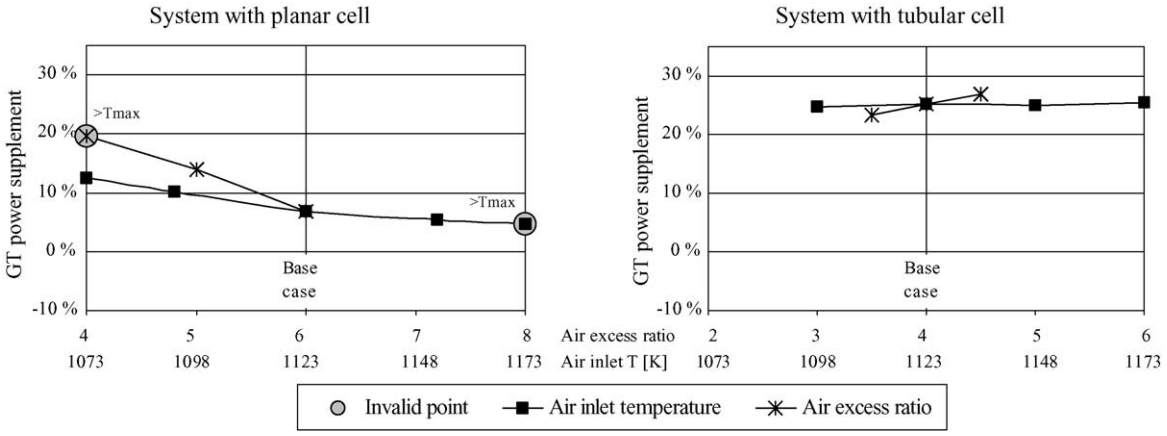

Fig. 9. Dependency of gas turbine power supplement on air inlet temperature and air excess ratio.

3.4. Near-optimum case

In accordance with preliminary studies, the pressure of the planar system has been reduced to 2 bar and the air inlet temperature of the tubular system is raised to 973 K in order to study a near-optimum case. Base case parameters have been assumed for the remaining values. For the planar system, the maximum local temperature in the cell is at its limit. Simulations with a combination of lower air inlet temperature and lower air excess ratio did not show significant efficiency improvements. Table 10 shows relevant operational data at the near-optimum point.

Fig. 10 displays charts for solid temperature, current density, hydrogen and methane of the planar fuel cell at near-optimum operation. The temperature distribution shows that the maximum local temperature occurs at the air outlet and near the fuel outlet. Close to the outlet of the fuel flow, temperature decreases due to decreasing electrochemical reaction

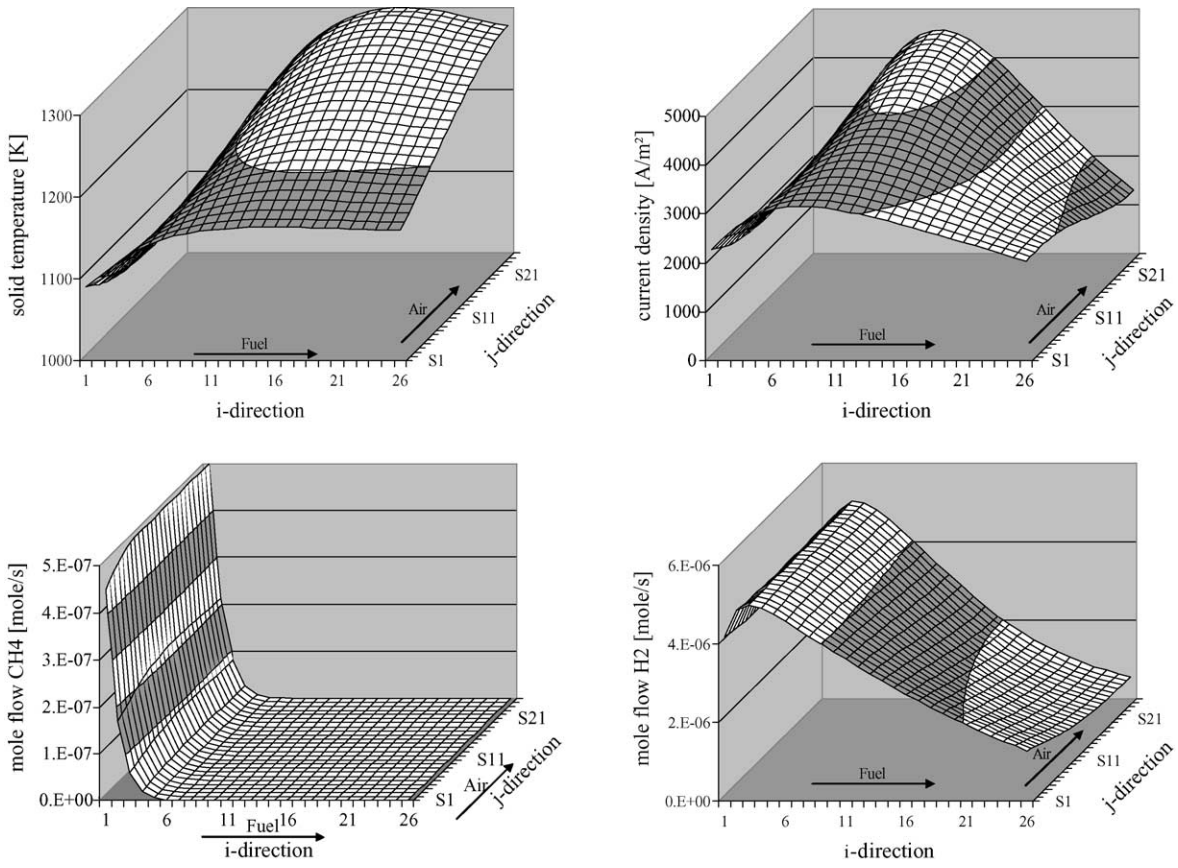

Fig. 10. Temperature, current density, H_2 and CH_4 molar flow fields for the planar cell at near-optimum case.

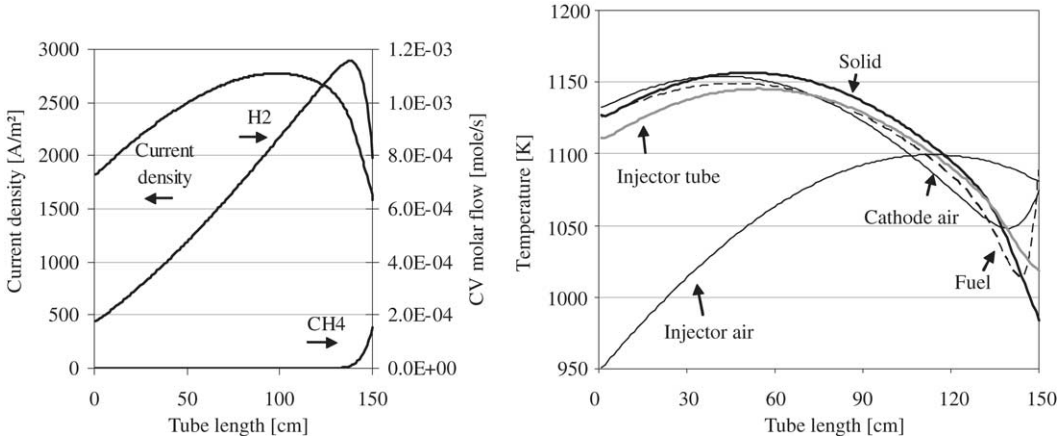

Fig. 11. Temperatures, current density, H_2 and CH_4 molar flow fields for the tubular cell at near-optimum case.

Table 10
Operational data at near-optimum case

System	Parameter	Planar system	Tubular system
Fuel cell	Efficiency (LHV, %)	62.5	54.7
	Voltage (V)	0.705	0.641
	Max. temperature (K)	1300	1175
GT cycle	TIT (K)	1191	1220
	Spec. turbine power[a] (%)	51	68
	Spec. compressor power[a] (%)	28	35
	Total efficiency (LHV, %)	66.9	66.7

[a] Ratio between power of compressor/turbine and fuel cell power.

rate, cooling by the air and the radiation to the pre-reformer. The figure also shows that most of the methane is reformed at the inlet. The hydrogen mole flow decreases steadily towards the fuel outlet. The current density as a measure for the electrochemical reaction is mainly influenced by the temperature (through the ohmic resistivity) and the amount of hydrogen (through the Nernst equation). Thus the maximum lies between the hydrogen and the temperature maximum.

Fig. 11 shows parameters in the tubular cell. The injector air flows to the right (downwards), while the reacting gases flow to the left (upwards) in these diagrams. It can be seen that the injector air is effectively cooling the cell in the upper section, while it provides some heat for the reforming reaction in the lower section. Hydrogen and methane mole flows and the current density behave similar to the planar model in *i*-direction.

4. Conclusions

The current paper describes two steady-state finite volume models for planar and tubular fuel cells. Although several simplifications and assumptions have been done during the development of the models, they provide reasonable results. This has been proven for the planar model by validation against the models from Selimovic [3] and Rechenauer [11]. A validation of the tubular model against Campanari [4] shows a certain divergence at high-pressure. However, no complete set of parameters from one source was found in literature, making a proper validation impossible.

It has been shown that hybrid systems can achieve efficiencies above 65% with the planar as well as the tubular geometry SOFC. The main difference between the planar and the tubular system for the gas turbine cycle is the internal pre-heating of the air in the tubular system, permitting a lower air inlet temperature. The thereby reduced amount of high-temperature heat in the pre-heating section allows for a higher-pressure ratio at acceptable turbine inlet temperatures. The tubular system's ability to be operated at lower air excess ratio lowers the exhaust gas losses and increases the afterburner temperature, improving the effectiveness of the GT cycle. These effects compensate for the lower efficiency of the tubular fuel cell stack, which is caused by its higher ohmic resistivity.

The introduction of additional fuel to the afterburner increases the turbine inlet temperature and therewith the GT cycle yield. The efficiency of both systems at higher pressures can be raised by this method. In case of the planar system, the power supplement of the GT cycle can be significantly increased. This effect could play a roll for the power output control of hybrid systems capable of pressure variation.

References

[1] H. Karoliussen, et al., SOFC stack modeling with internal reforming, in: Proceedings of the fourth IEA Workshop on SOFC, Lausanne, Switzerland, August, 1992.
[2] K. Hassmann, SOFC power plants, the Siemens–Westinghouse approach, Fuel Cells 1 (2001) 1.
[3] A. Selimovic, SOFC Modelling for SOFC/GT Combined Cycle Simulations, Licenciate Thesis, Lund University, Sweden, 2000.
[4] S. Campanari, P. Iora, Definition and sensitivity analysis of a finite volume SOFC model for a tubular cell geometry, J. Power Sources 132 (2004) 113–126.
[5] U.G. Bossel, Final Report on SOFC Data, Facts and Figures, Swiss Federal Office of Energy, Berne, 1992.

[6] K. Nisancioglu, Natural Gas Fuelled Solid Oxide Fuel Cells and Systems, Swiss Federal Office Of Energy, 1989, p. 96.
[7] T. Ota, M. Koyama, C. Wen, K. Yamada, H. Takahashi, Object-based modeling of SOFC system: dynamic behavior of micro-tube SOFC, J. Power Sources 5249 (2003) 1–10.
[8] W.M. Rohsenow, J.P. Hartnett, Y.I. Cho, Handbook of Heat Transfer, third ed., McGraw-Hill, 1998.
[9] H. Yakabe, et al., 3-D model calculation for planar SOFC, J. Power Sources 102 (2001) 144–154.
[10] F.P. Incropera, D.P. Dewitt, Fundamentals of Heat and Mass Transfer, fifth ed., Wiley and Sons Inc., 2002.
[11] C. Rechnenauer, E. Achenbach, Dreidimensionale mathematische Modellierung des stationären und instationären Verhaltens oxidkeramischer Hochtemperatur-Brennstoffzellen, Doctoral Thesis, Forschungszentrum Jülich, Germany, 1993.
[12] G. Engeln-Muellges, F. Uhlig, Numerical Algorithms with C, Springer-Verlag, 1996.
[13] E. Achenbach, International Energy Agency, Annex II, Modelling and Evaluation of Advanced SOFC, Subtask A: Numerical Modelling, Experimental Data Base and Validation, Activity A2: Stack Modelling, 1995.
[14] J. Pålsson, Thermodynamic Modelling and Performance of Combined SOFC and GT Systems, Doctoral Thesis, Lund University, Sweden, 2002.
[15] Y. Yi, T.P. Smith, J. Brouwer, A.D. Rao, G.S. Samuelsen, Simulation of a 220 kW hybrid SOFC gas turbine system and data comparison, in: Proceedings of the Electrochemical Society, vol. 7, 2003.